Journal of Inorganic Biochemistry 200 (2019): 110805
DOI: https://doi.org/10.1016/j.jinorgbio.2019.110805

Multifunctional coordination polymers based on copper with modified nucleobases easily modulated in size and conductivity.

Verónica G. Vegas[a], Noelia Maldonado[a], Oscar Castillo[b], Carlos J. Gómez-García[c] and Pilar Amo-Ochoa* [a,d]

Supporting Information

Table S1. Single-crystal data and structure refinement details for compounds **CP1**, **CP2** and **CP3**

	CP1	**CP2**	**CP3**
Empirical formula	$C_{26}H_{28}Cu_2N_6O_{15}$	$C_{24}H_{22}Cu_2N_6O_{14}$	$C_{24}H_{22}Cu_2N_6O_8$
M_r	791.62	745.55	649.55
T/K	293(2)	200(2)	296(2)
Crystal system	Triclinic	Triclinic	Triclinic
Space group	$P\bar{1}$	$P\bar{1}$	$P\bar{1}$
a/Å	4.7318(4)	4.7559(3)	4.9333(1)
b/Å	11.4783(7)	10.3952(7)	9.7064(2)
c/Å	14.9644(12)	14.6613(10)	13.1365(3)
α/º	101.729(4)	95.604(2)	73.895(1)
β/º	97.044(5)	94.876(2)	82.707(1)
γ/º	93.752(4)	91.631(2)	89.008(1)
V/Å^3	786.36(10)	718.26(8)	1348.68(14)
Z	1	1	1
D_c/Mg·m^{-3}	1.672	1.724	1.800
Color	Blue-green	Green	Yellow
Crystal habit	Prismatic	Needle	Prismatic

Crystal size/mm^3	0.31 x 0.14 x 0.06	0.22 x 0.03 x 0.02	0.26 x 0.08 x 0.04
μ/mm^{-1}	1.435	1.562	1.840
$2\theta_{max}$/º	50.70	50.70	50.70
Reflections collected	22072	10468	19698
Independent reflections	2882	2623	2185
R_{int}	0.0533	0.0302	0.0330
Variable parameters	219	208	182
$R1$[I>2σ(I)]/$wR2$[all data][a]	0.0413/0.1127	0.0286/0.0655	0.0238/0.0670
Goodness-of-fit (F^2)	1.085	1.068	1.107
$\Delta\rho_{max/min}$/e Å^{-3}	1.258, -0.588	0.539, -0.295	0.295, -0.418

[a] $R1 = \Sigma\,||F_o| - |F_c||\,/\,\Sigma\,|F_o|$; $wR2 = [\Sigma[w(F_o^2 - F_c^2)^2]\,/\,[\Sigma(F_o^2)^2]]^{1/2}$ where $w = 1/[\sigma^2(F_o^2)+(AP)^2+(BP)]$ with A = 0.0504 (**CP1**), 0.0201 (**CP2**), 0.0508 (**CP3**); and B = 1.5693 (**CP1**), 0.9108 (**CP2**), 0.5724 (**CP3**).

Table S2. Selected bond lenghts (Å) and angles (º) for compounds CP**1** and CP**2**.[a]

	CP1 (X=9)	**CP2** (X=8)		**CP1** (X=9)	**CP2** (X=8)
Cu1-N21	1.995(3)	1.9736(19)	Cu1-OX1	1.942(2)	1.9459(17)
Cu1-O11	1.979(3)	1.9966(17)	Cu1-OX2	2.737(2)	2.7733(17)
Cu1-O12^{9}	2.001(2)	1.9954(17)	Cu1-OX2^{ii}	2.196(2)	2.1827(16)
Cu1···Cu1^{i}	5.2098(9)	5.2095(6)	Cu1···Cu1^{iii}	11.0685(11)	11.0280(9)
Cu1···Cu1^{iv}	4.7318(4)	4.7559(3)			
N21-Cu1-O11	90.51(11)	90.73(8)	O11-Cu1-OX2^{ii}	93.41(11)	92.86(7)
N21-Cu1-O12^{i}	168.77(12)	166.62(8)	O12i-Cu1-OX1	91.50(10)	92.46(7)
N21-Cu1-OX1	93.47(11)	91.50(8)	O12i-Cu1-OX2	89.57(10)	92.43(6)
N21-Cu1-OX2	85.41(11)	79.91(7)	O12i-Cu1-OX2^{ii}	92.58(11)	91.85(7)
N21-Cu1-OX2^{ii}	97.11(11)	100.56(7)	OX1-Cu1-OX2	52.92(8)	52.44(6)
O11-Cu1-O12^{i}	83.22(10)	83.59(7)	OX1-Cu1-OX2^{ii}	94.07(9)	94.78(7)
O11-Cu1-OX1	171.03(11)	171.51(7)	OX2-Cu1-OX2^{ii}	146.98(11)	147.09(8)
O11-Cu1-OX2	119.55(10)	92.43(6)			

[a]Symmetry codes for **CP1**: (i) -x+1, -y, -z+1; (ii) x+1, y, z; (iii) –x+1, -y, -z+2; (iv) x+1, y, z. Symmetry codes for **CP2**: (i) -x+1, -y+1, -z+1; (ii) –x+2, -y+1, -z+1; (iii) x-1, y-1, z; (iv) x+1, y, z.

Table S3. Hydrogen bonding interactions in compounds **CP1** and **CP2**.[a]

	CP1			CP2		
D–H···A[b]	H···A	D···A	D–H···A	H···A	D···A	D–H···A
N3–H3···O2[i]	1.99	2.843(5)	173	2.05	2.928(3)	175
C23–H23···O4[ii]	2.40	3.333(5)	177	2.32	3.269(3)	179
C25–H25···O4[iii]	2.24	3.170(5)	173	2.25	3.194(3)	176

[a]Symmetry codes for **CP1**: (i) –x+1, -y+1,-z+2; (ii) x-1, y-1, z; (iii) -x+2, -y+1. Symmetry codes for **CP2**: (i) -x, -y, -z; (ii) x-1, y+1, z; (iii) -x+1, -y, -z.

[b] D = donor; A = acceptor.

Table S4. Selected bond lenghts (Å) and angles (º) for compound **CP3**.[a]

Cu1-N11	1.898(2)	N11-Cu1-O91	152.99(8)
Cu1-O91	1.971(2)	N11-Cu1-O91[i]	127.12(8)
Cu1-O91[i]	2.133(2)	O91-Cu1-O91[i]	78.60(7)
Cu1···Cu1[ii]	3.0256(7)	Cu1···Cu1[iii]	10.9017(6)

[a]Symmetry codes: (i) -x+1, -y+1, -z+1; (ii) -x, -y+1, -z+1; (iii) -x-1, -y, -z+1.

Table S5. Structural parameters (Å, º) of more relevant noncovalent interactions in **CP3**.[a]

Hydrogen-bonding interactions			
D–H···A[b]	H···A	D···A	D–H···A
N3–H3···O2	1.97	2.823(2)	175
C13–H13···O4[ii]	2.41	3.323(3)	168
C15–H15···O4[iii]	2.41	3.322(3)	166
C16–H16···O2[iv]	2.46	3.327(3)	156

π-π interactions	Angle	DC	DZ	DXY	Dist.

Ring···Ring[c,d]			α			
Thym-Thym[iv]	0.0	3.93	35.5	3.20	2.29	3.22–3.47

[a]Symmetry: (i) –x+2, -y+1, -z; (ii) x-1, y-1,z-1; (iii) –x+1, -y+1, -z+1; (iv) –x+2, -y+1, -z+1; (v) –x+1, -y+1, -z.

[b] D = donor; A = acceptor.

[c]Angle: dihedral angle between the planes (°), DC: distance between the centroids of the rings (Å), α: angle between the normal to the first ring and the DC vector (°), DZ: interplanar distance (Å), DXY: lateral displacement (Å), Dist: shortest distances between the non hydrogenoid atoms of both rings (Å).

[d]Thym: ring of the thymine residue.

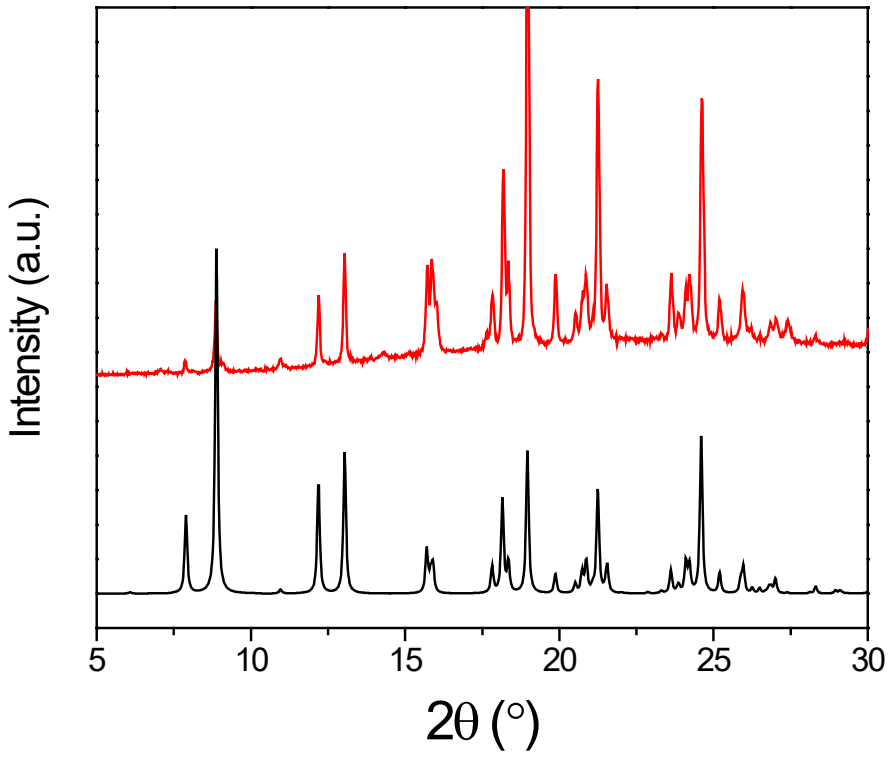

Figure S1. PXRD patterns of **CP1**. Red line corresponds with the experimental data and black line corresponds with simulated data.

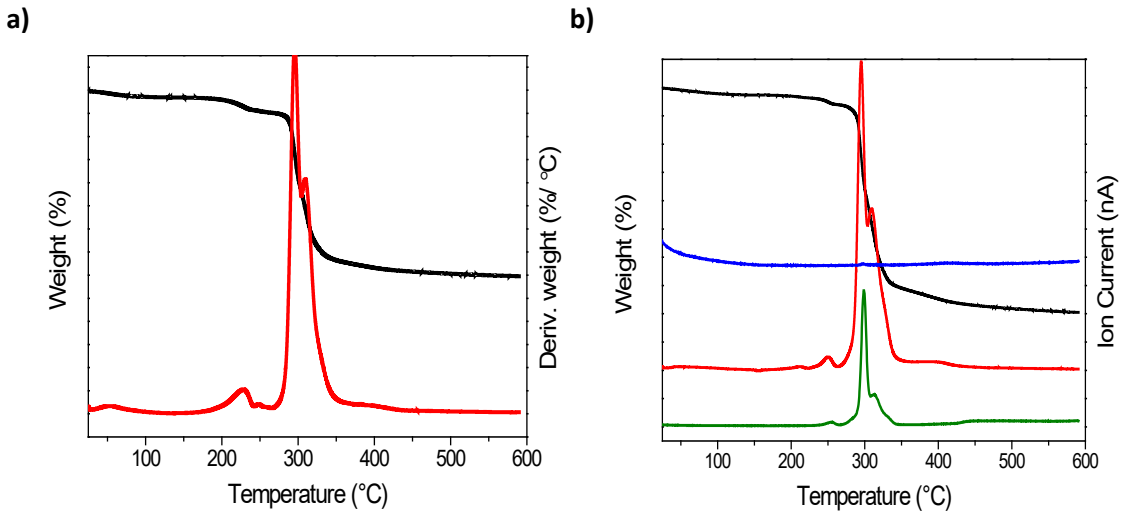

Figure S1. Thermal stability of **CP1** (a) and Thermal stability of **CP1** previously dehydrated to 140 °C (b). Thermogram signals: black and red line (weight and derivated weight, respectively) represent the stages of the losses produced; green and blue line represent the ion currents corresponding to the mass 18 (blue) and 44 (red).

Its thermal study (Fig. S1 (a)), shows a 1st stage at 135 °C probably indicative of the loss of insterstitial water molecules (obsd 4.3 %, calcd 4.45 %). The following stages correspond with the loss of oxalate, 4,4'-bpy and two $TAcO^-$ molecules, in this order, from 140 °C to 650 °C.
In Figure S1 (b) the ionic current indicates that there is not water (m/z=18) at 135 °C compared to the previous graphic, due to its heat treatment at 140 °C before analysis. Also, we can observe how the oxalate, 4,4'-bipy and $TAcO^-$ are lost as CO_2 (m/z= 44).

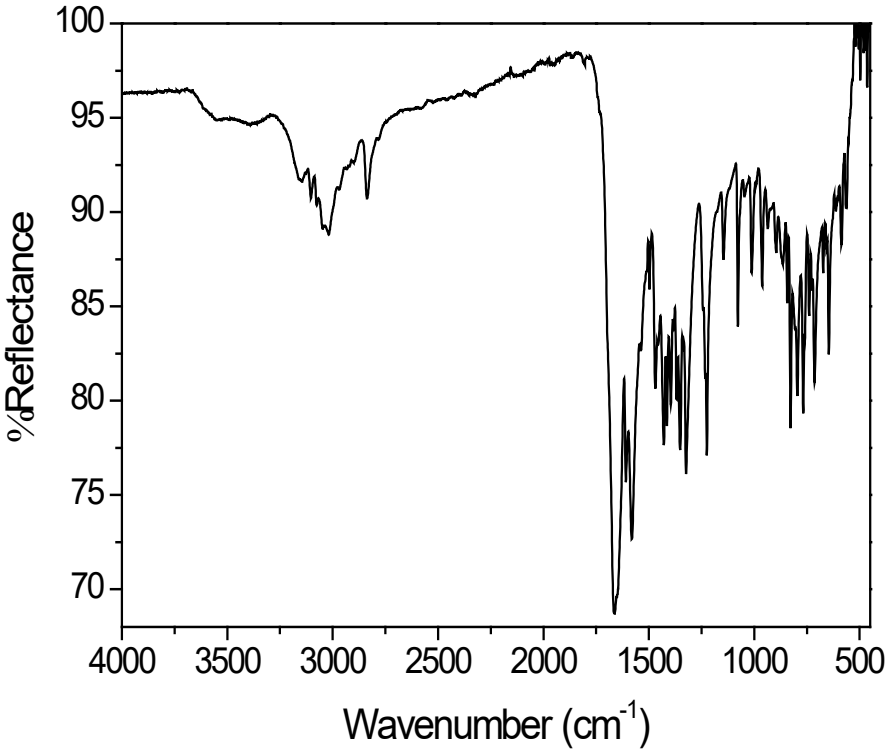

Figure S3. ATR-FT-IR spectrum of **CP1**.

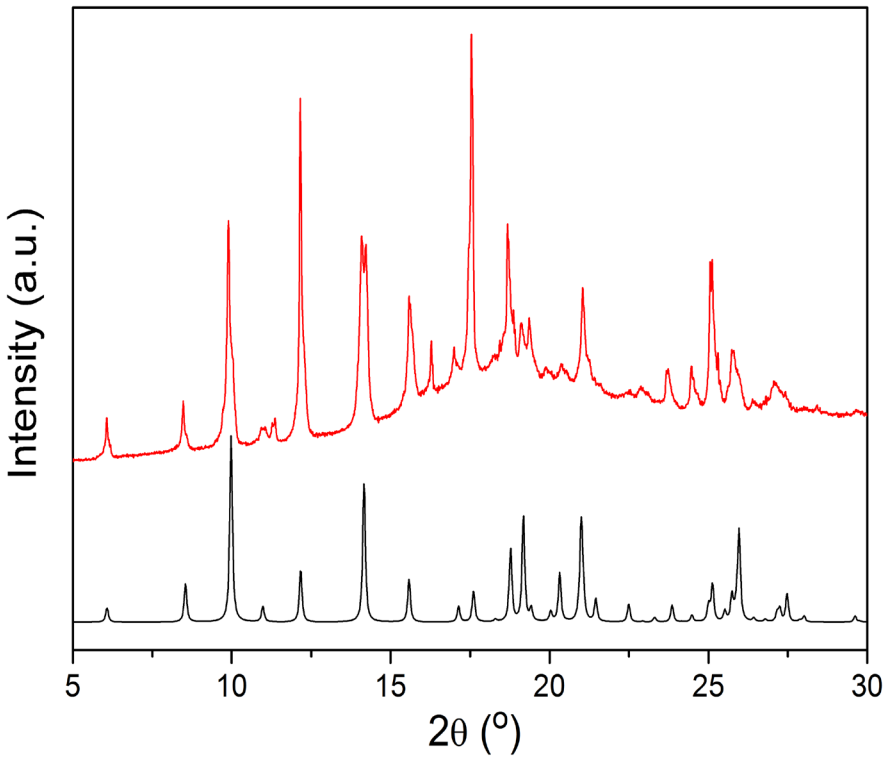

Figure S4. PXRD patterns of **CP2** (red line) and simulated data (black line).

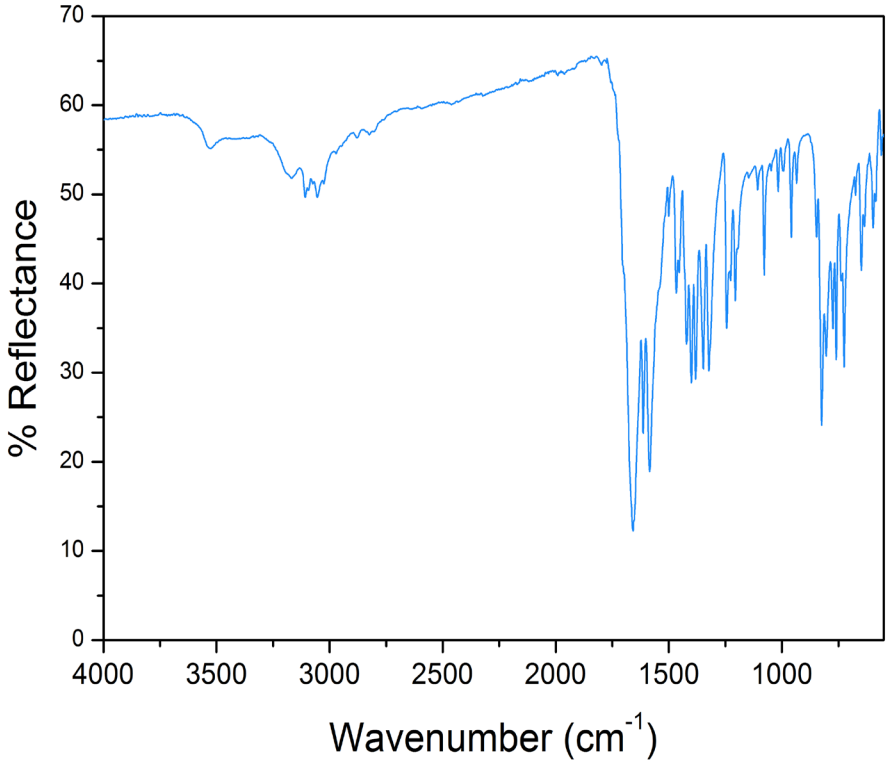

Figure S5. ATR-FT-IR spectrum of **CP2**.

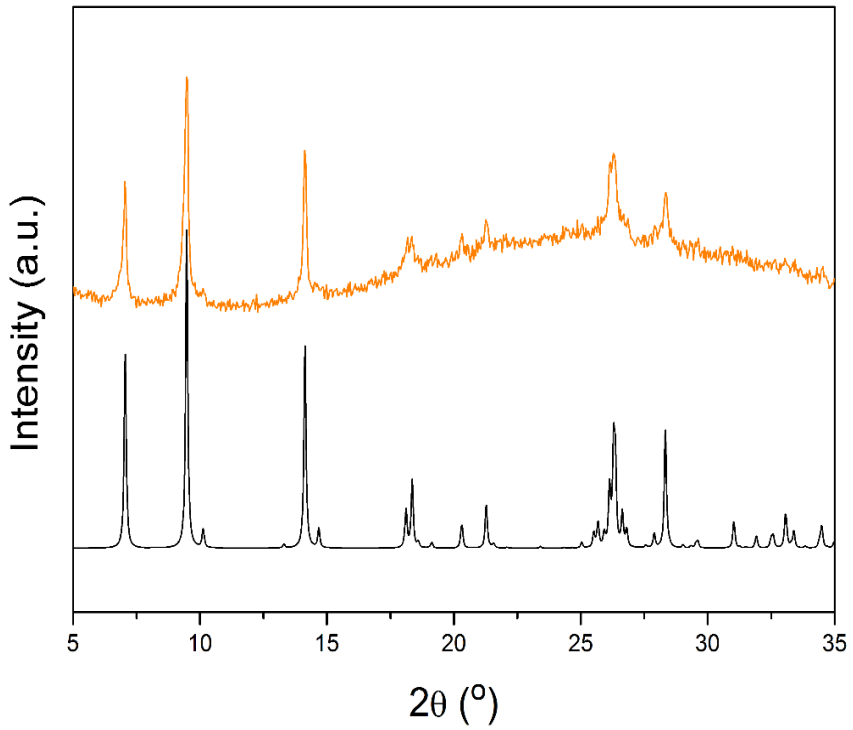

Figure S6. PXRD patterns of **CP3** (orange line) and simulated data (black line).

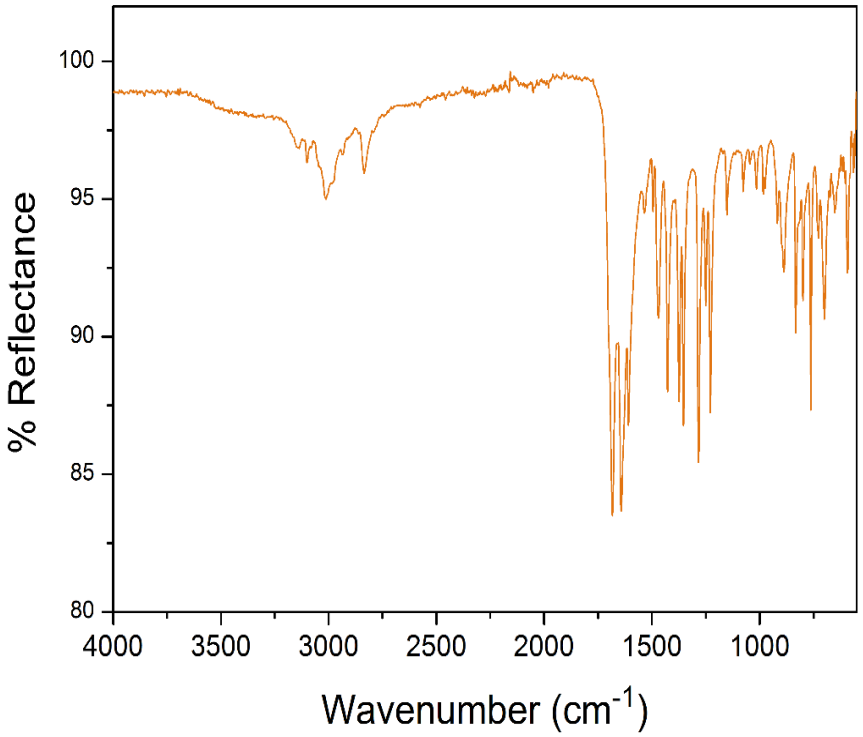

Figure S7. ATR-FT-IR spectrum of **CP3**.

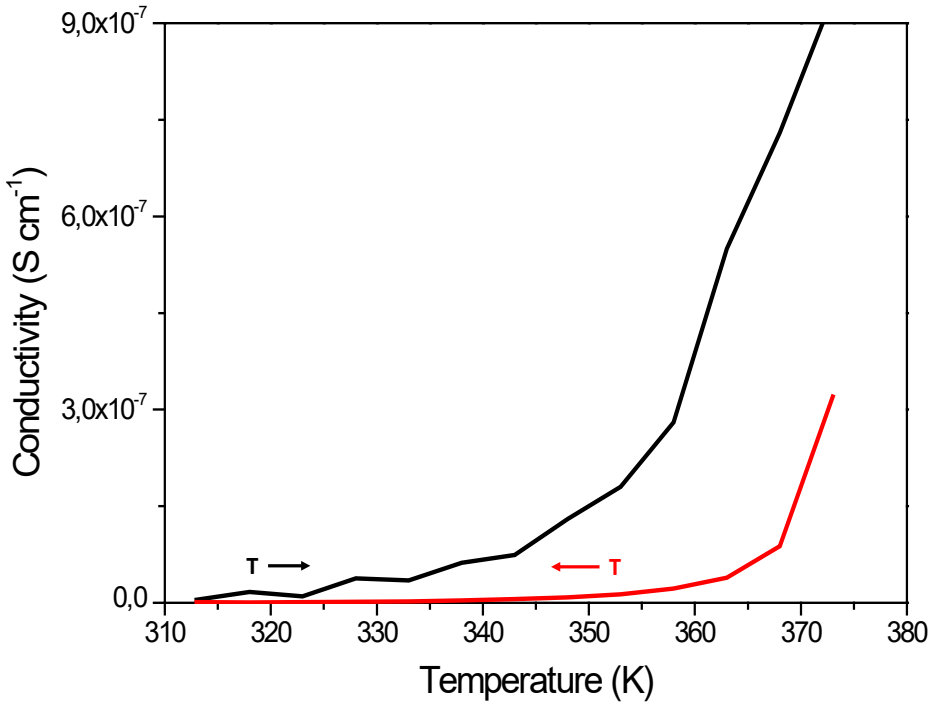

Figure S8. Conductivity variation of **CP1** during heating (black) and cooling (red).

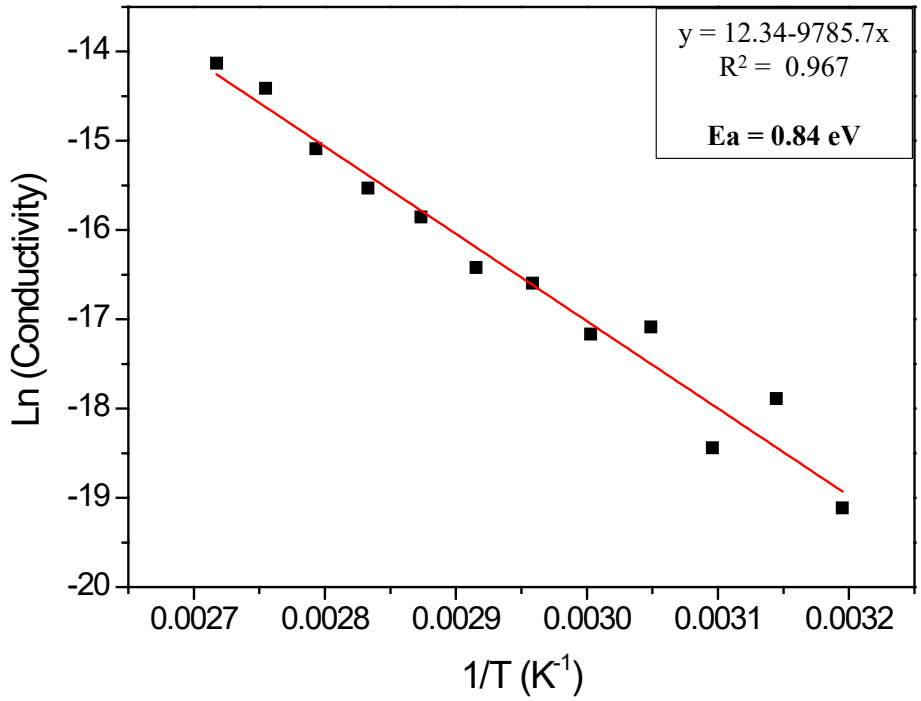

Figure S9. Linear fitting of Ln (Conductivity) versus 1/T to calculate the activation energy (Ea) in **CP1**, according to the Arrhenius Equation.

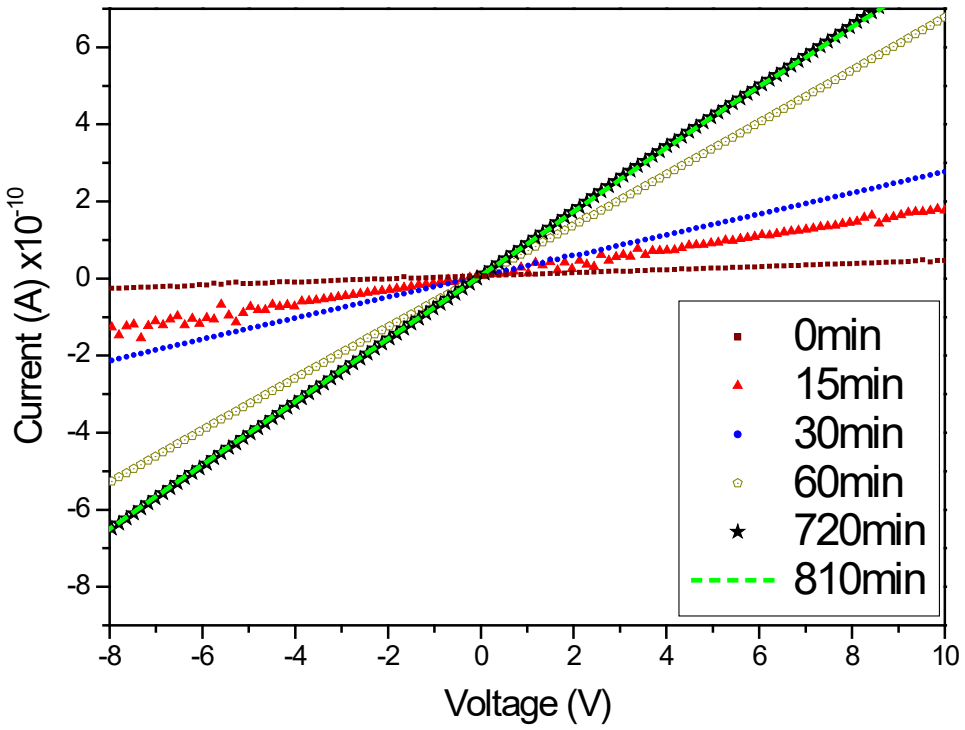

Figure S10. Variation of current versus voltage in **CP1** when it has been doped with I_2 from 0 to 810 minutes.

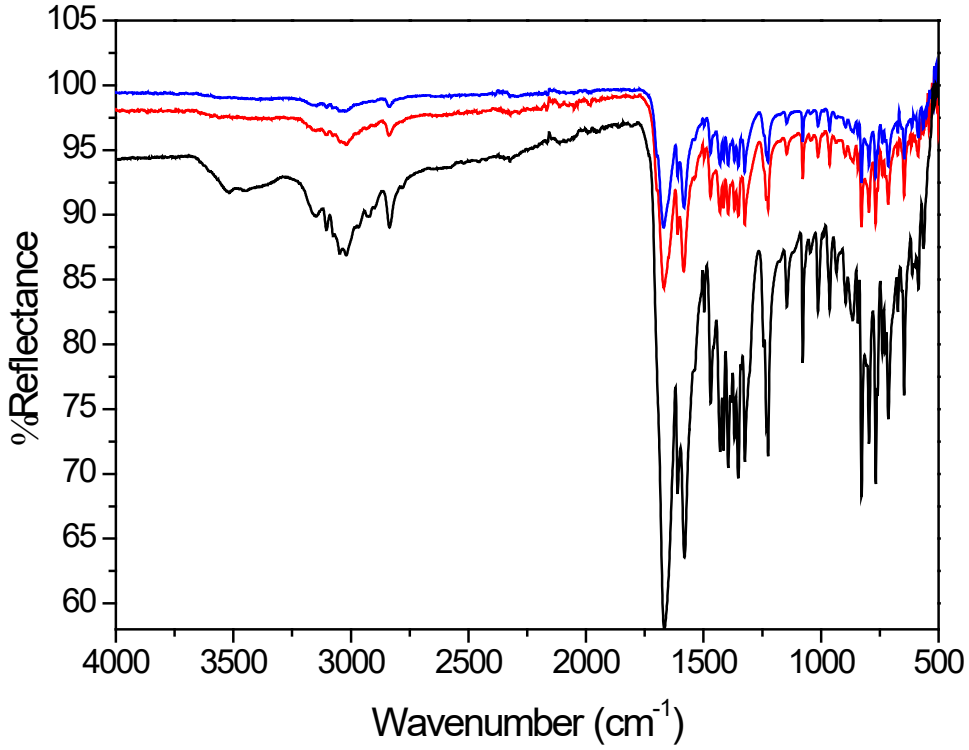

Figure S11. ATR-FT-IR spectra of **CP1** (black line), **microCP1** after sonication (blue line) and **nanoCP1** (red line) after centrifugation.